JOURNAL OF Materials CHEMISTRY

The preparation of chromium, nickel and chromium–nickel alloy nanoparticles on supports

Richard D. Tilley*† and David A. Jefferson

Department of Chemistry, University of Cambridge, Lensfield Road, Cambridge, UK CB2 1EW

Received 16th May 2002, Accepted 20th August 2002
First published as an Advance Article on the web 12th September 2002

Chromium, nickel and chromium–nickel alloy nanoparticles have been synthesised *via* the addition of a metal salt solution to a support, followed by drying and reduction with hydrogen at elevated temperatures. Chromium and chromium–nickel alloy particles were prepared using ethylene glycol solutions and were found to be stable on silica and baddeleyite (ZrO_2) supports. The crystal structures adopted were investigated using high resolution electron microscopy (HRTEM) and found to be similar in both cases to the bulk metal and alloy. The particle morphology, also from HRTEM observations, was found to be pseudo-spherical. Nickel nanoparticles could be formed using an aqueous solution on a variety of supports and were found from powder X-ray diffraction (PXRD) and HRTEM data to adopt the face-centred cubic structure of the bulk metal. The effect of different supports on the average particle size was investigated with PXRD and the particle morphology with HRTEM. The supports were found to have little effect on the average particle size, but had a noticeable influence on morphology, with particles on alumina being found to be flat and angular in contrast to those on graphitised carbon and ceria, which had pseudo-spherical morphologies.

Introduction

Research involving transition metal nanoparticles has been extensive due to their applications as catalysts. It has recently been shown that metal nanoparticles of Co,[1,2] Ni[3] and Pd[4] adopt different structures to those of bulk metals. These different structures form because of the large fraction of atoms that are situated at or close to the surface of the particle. To date, the majority of previous metal nanoparticles investigations have focussed on the group 10 and 11 metals, nickel, palladium and platinum, and copper, silver and gold. Nanoparticles of metals from these groups are relatively easy to synthesise and are stable once formed. In this work, nickel-supported catalysts have been have synthesised because of their possible applications in many industrially important processes, such as hydrogenation,[5] methylation,[6] steam reforming[7] and hydrocracking,[8] and to compare their structures and morphologies with the chromium and chromium–nickel particles also prepared. Several supports have been used in previous nickel metal nanoparticle investigations, these include silica,[5,9–12] carbon encapsulation,[13] alumina[14] and zeolites.[8,15–17] In this study, high resolution electron microscopy (HREM) was used to compare the morphology of nickel nanoparticles on supports of graphitised carbon, in the form of Carbopack (carbon black), ceria (CeO_2) and γ-alumina.

The solution synthesis of nanoparticles of transition metals to the left of the Periodic Table, such as chromium, has been rather limited, with the recent report of the production of TOPO-capped chromium particles by Green and O'Brien[18] being a notable exception. Furthermore, research involving alloy nanoparticles is even scarcer, excepting the detailed work on FePt[19] and FeCo,[1] which have been studied because of their magnetic properties. It was thus decided to see if, by modifying the synthetic route used to make the nickel particles, whether chromium and chromium–nickel particles could also be produced. By changing the solvent and the temperature necessary to effect the reduction, chromium and chromium–nickel nanoparticles have been synthesised for the first time from solution on supports. As with the nickel particles, the structures adopted were compared with those of the bulk materials and the particle morphology analysed to see if there was an observable effect from the support.

Methods

Nickel nanoparticles were prepared from nickel nitrate $Ni(NO_3)_2{\cdot}6H_2O$ (Fisons, 99.9% purity) dissolved in the minimum amount of distilled water and loaded onto a support. Two sets of experiments were performed, the first using Carbopack (Supelco) as the support, with the metal molar loading being varied from 10 to 50%. A second set of experiments used a 50% molar loading on Carbopack, γ-alumina (γ-Al_2O_3, Johnson and Matthey, 99.99%), and ceria (CeO_2, Alfa, 99.99% purity) supports. Each sample was heated in an oven at 100 °C for 24 h to remove the solvent and reduced at 300 °C for 3 h in a hydrogen atmosphere. After the reaction, samples were allowed to cool for 20 min in the furnace whilst the gas was still flowing and only removed when the temperature was below 70 °C to minimise any possible oxidation of the specimen.

Any attempt to prepare chromium nanoparticles from aqueous solution invariably resulted in the production of oxide particles, presumably due to a reaction with remaining water during the drying process. This is described in more detail below. Consequently, they were synthesised from chromium nitrate dissolved in the minimum amount of ethylene glycol and loaded onto a support. A strong reaction occurred with Carbopack supports on reduction, resulting in greatly increased graphitisation of the support, and the only stable preparations utilised either silica (SiO_2, BDH precipitate, acid washed) or baddeleyite (ZrO_2, Koch Light Ltd., 99.8% purity) as the supporting medium. A 50% molar metal loading was prepared with typically 0.50 g of support used. The sample was dried in an oven at 100 °C for 24 h and then reduced at

†Present address: Advanced Materials Laboratory, Toshiba RDC Center, 1, Komukai Toshiba-Cho, Saiwai-ku, Kawasaki 212-8582, Japan. E-mail: richard.tilley@glb.toshiba.co.jp.

600 °C for 6 h with hydrogen. Samples of chromium–nickel alloy nanoparticles on a silica support were prepared with analogous conditions to the chromium metal particles using metal ratios of 2 Ni : 1 Cr, 1 Ni : 1 Cr and 1 Ni : 2 Cr. The preparations were then reduced with hydrogen in a furnace at 600 °C for 6 h.

Preliminary characterisation of all samples was *via* X-ray powder diffraction using a STOE diffractometer with a horizontal goniometer and Cu-Kα radiation (λ = 0.1542 nm). Where peaks due to metal particles could be identified, particle size analysis using the Scherrer equation was carried out. Specimens for electron microscopy were prepared directly from the product material by suspension in acetone and transferring to a gold grid coated with an amorphous carbon support. HRTEM images were recorded on a JEOL JEM-3011 electron microscope with a LaB_6 cathode operated at 300 keV. Images were recorded photographically at magnifications ranging from 3 to 600 000 ×, and were then digitised for subsequent analysis. Digital image processing and fast Fourier transform formation was performed using Semper 6+ software. Computer-simulated electron diffraction patterns were obtained from CaRIne 3.1 software (ESM Software, Hamilton, OH, USA). The JEM-3011 was fitted with a PGT-XS14 energy dispersive X-ray (EDX) detector and AVALON associated analytical system. Calibration of detector sensitivity for Cr-Kα and Ni-Kα radiation was effected by use of the bulk sulfide $NiCr_2S_4$, which was confirmed as single phase by X-ray powder diffratometry.

Identification of individual nanoparticles in the electron microscope using nanobeam diffraction techniques proved impractical, partly due to rapid contamination of the specimen when the microscope was being used in nanobeam mode, but also because of the very high background diffraction from the supporting medium, which made the diffraction pattern of the particles difficult to resolve. Particle characterisation was therefore achieved by obtaining a power spectrum from a fast Fourier transform of the high resolution lattice fringe images, which had the advantage, particularly in the case of amorphous silica supports, that the resulting pattern contained little contribution from the support. The power spectrum was then compared to a simulated diffraction pattern from a model of the specimen under analysis.

To identify the nanocrystals observed in electron micrographs, it was necessary to measure the lattice fringes on the particles to a high degree of precision. This was due to the difficulty found in distinguishing between metal and metal oxide, stemming from the fact that energy dispersive X-ray spectroscopy for particles on an oxide support invariably produced an oxygen signal from the latter. Use of the power spectrum was preferred to actual measurement of fringe spacings in the image, since it was intrinsically more accurate and avoided the parallex errors invariably present in measurement of fringe spacings manually. Calibration of the spacing between lattice fringes on the nanocrystals was obtained by comparison with the known spacings of the graphitised carbon, ceria or baddeleyite support. For experiments on amorphous silica and partially crystalline alumina supports, gold nanoparticles were added to the specimen when examined in the electron microscope. Gold nanoparticles can be easily distinguished from the sample nanoparticles either by EDX or from the image, as they are often multiply twinned. They display fringes with lattice spacings of 0.236 nm from the (111) planes and 0.204 nm from the (200) planes, which were used to calibrate the lattice fringes on the specimen nanocrystals. An attempt was made to distinguish between metal and oxide particles using image simulation methods, but images of metal and metal oxide were almost identical at the point resolution of the microscope used (0.17 nm), apart from their dimensions, and the method proved to be of little value in characterisation.

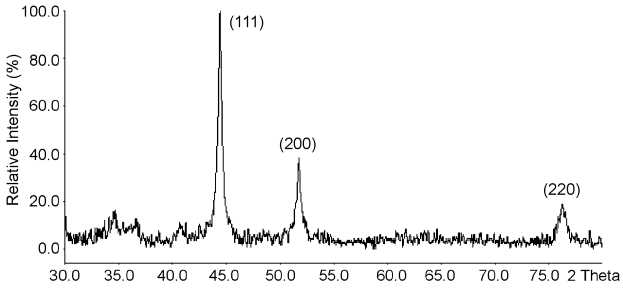

Fig. 1 The powder X-ray diffraction pattern of a 30% loaded sample of nickel metal particles on a Carbopack support. Peaks show broadening due to the small particle size.

Results and discussion

Nickel nanoparticles

In the first set of experiments, nickel metal particles were prepared on a Carbopack support with a range of metal molar loadings ranging from 10–50%. The peaks in each of the powder X-ray diffraction patterns recorded can be indexed to face-centred cubic nickel metal. The pattern for the 30% loaded sample is shown in Fig. 1 and is a typical representation of those obtained. The average particle size for each loading was calculated by applying the Scherrer equation to the peak broadening and the results, as summarised in Table 1, indicate that the more heavily loaded samples had a greater average particle size, with a 23.5% increase for a change of loading from 10 to 30% and a 35% increase for a change of loading from 10 to 50%. These finding are more in accordance with those of Estournez *et al.*,[10] who reported only a 14% increase in average particle size with a change in loading from 10 to 21%, rather than those of Ueno *et al.*,[5] who found an approximate size increase of 50% when going from a 10 to 25% loading. It must be noted that in both of these studies the particles were made on a silica support, not graphitised carbon, and the discrepancy between their findings was attributed to the differences in the elaboration process.[10]

In the second set of experiments, three samples were synthesised on Carbopack, alumina and ceria supports, each with a 50% molar loading. The average particle sizes for each support obtained from X-ray diffraction data and summarised in Table 2 were found to be very similar for all samples, indicating little influence from the support in this respect. Electron microscopy showed that there was a large variation in particle size, ranging from 2 to 50 nm for all sample loadings and supports. Nanocrystals on the Carbopack and ceria supports were observed to be pseudo-spherical, and the micrograph shown in Fig. 2 shows a typical group of nickel nanoparticles on a Carbopack support. In contrast, HRTEM

Table 1 The average nickel nonoparticle size for 10, 30 and 50% molar loadings, calculated using the Scherrer equation

Loading (%)	Average particle size/nm
10	17 +/−2
30	21 +/−2
50	23 +/−2

Table 2 The average nickel nanoparticle size for 50% molar loadings on Carbopack, ceria and alumina supports, calculated using the Scherrer equation

Support	Average particle size/nm
Carbopack	23 +/−2
Ceria	25 +/−3
Alumina	22 +/−2

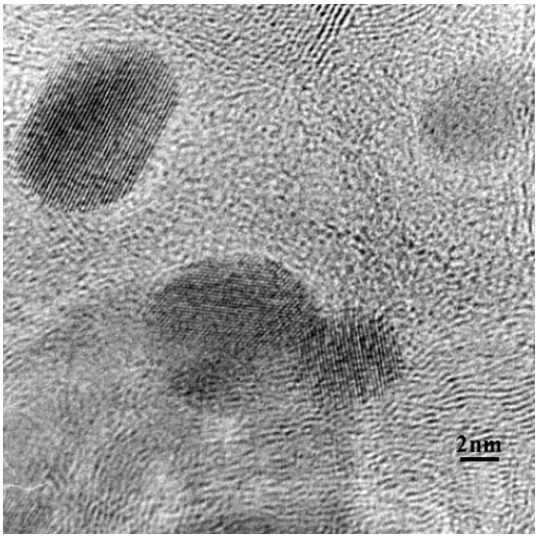

Fig. 2 An HRTEM image of a typical group of nickel nanoparticles on a Carbopack support.

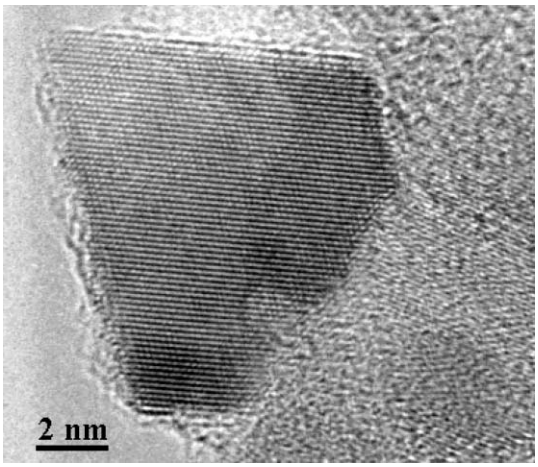

Fig. 3 An HRTEM image of a 10 nm angular nickel nanoparticle on an amorphous alumina support.

studies of nickel nanoparticles on alumina showed that the crystallites were thin and formed with sharp, angular faces, a typical nanocrystal being shown in Fig. 3. Previous studies of metal–support interactions have shown that nanocrystals of nickel and platinum metals produced on supports which exert a strong metal–support interaction can adopt non-spherical morphology. For example, one of the earliest reports was by Mustard and Bartholomew in 1981,[20] in which nickel particles on TiO_2 were observed to have 'raft'-like morphologies. These crystals are characterised by their non-spherical shape, thinness and low contrast in electron microscope images. The particles formed on alumina in this study appear to take this form. A previous report on metal–support interactions ordered the strength of the interaction of several supports as $TiO_2 > Al_2O_3 > SiO_2$/carbon.[21] The particles synthesised on ceria in this study had a spherical morphology, suggesting that its strength of metal–support interaction is comparable to that of SiO_2 and carbon.

Chromium nanoparticles

Initial experiments aimed at synthesising chromium nanoparticles used distilled water as the solvent. However, as described earlier, it was found that Cr_2O_3 rather than the chromium metal nanoparticles were produced. It was suspected that chromium hydroxide was forming when the chromium nitrate was dissolved because the sample had a gelatinous character common with transition metal hydroxides. Upon subsequent reaction with hydrogen, the hydroxide only produced Cr_2O_3 and not chromium metal. In order to prevent possible hydroxide formation, subsequent experiments were performed using the non-aqueous solvent ethylene glycol. Ethylene glycol was found to dissolve chromium nitrate and, when it was evaporated, the residual sample was powdery and not gelatinous. Because of reaction with Carbopack, only two different supports, amorphous silica and baddeleyite, were used, and the samples were reduced in a furnace at 600 °C for 6 h with hydrogen.

Characterisation of nanocrystals in electron microscope images for the silica sample, such as the one shown in Fig. 4, using the method described in the previous section, indicated the successful formation of chromium metal nanoparticles. Chromium metal nanoparticles were also synthesised on a baddeleyite support and a typical particle is shown in Fig. 5. Images of particles on a baddeleyite support could be calibrated from the lattice fringes observed in the support. In both cases, the structure adopted was the body-centred cubic type of the bulk metal. From electron microscope observations of over 50 particles, the average metal particle size for both supports was found to be approximately 15 nm, with a size distribution of 2 to 30 nm. For both supports, the particle morphology found was to be pseudo-spherical, with no obvious effect from the supports on the particle shape observed by HRTEM. In both samples, approximately 10% of the nanoparticles examined had lattice fringe spacings which were too large for chromium metal and several of these were identified as Cr_2O_3 from electron micrographs. This co-existence of metal and metal oxide suggested that two deposition processes were occurring, which was further investigated

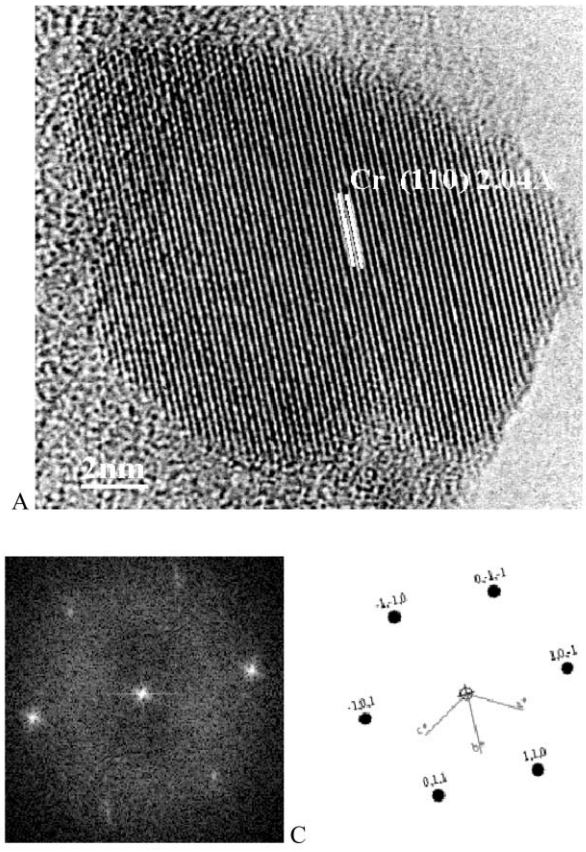

Fig. 4 An HRTEM image of a 14 nm chromium metal nanoparticle on an amorphous SiO_2 support (A). The power spectrum (B) from the chromium metal nanoparticle matches the simulation of the power spectrum (C) of b.c.c. chromium metal projected down the [111]. Spots are observable in the power spectrum from fringes that are not readily evident on the particle.

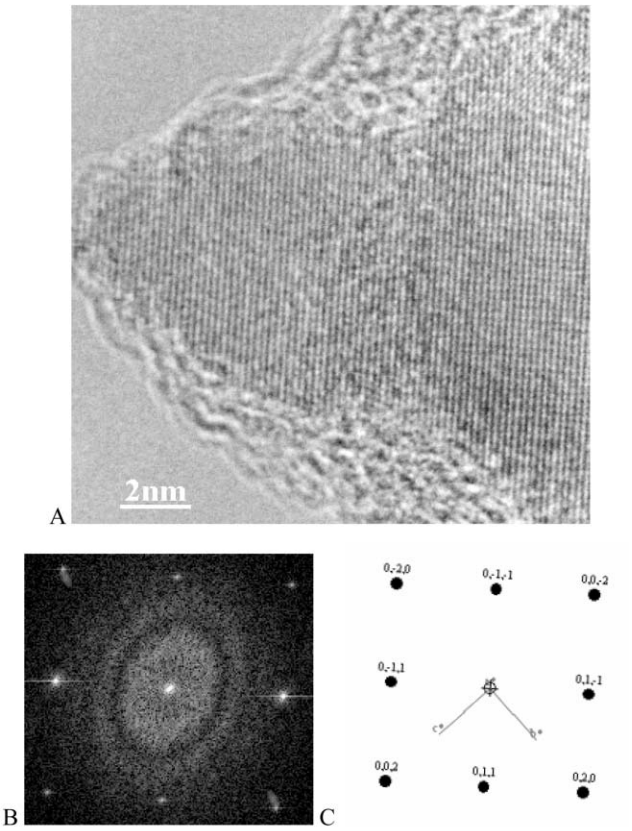

Fig. 5 An HRTEM image of a 22 nm chromium metal nanoparticle on a ZrO_2 support (A) with an amorphous coating. The power spectrum (B) and matching simulation (C) is of b.c.c. chromium metal projected down the [100].

by EDX. Although metal and oxide could not be distinguished directly, EDX spectra from areas of the silica support where no particles were present also showed the presence of chromium, suggesting that, in addition to some initial surface deposition as the oxide, chromium was also being absorbed by the support and partly re-emerging as metal in the reduction process. This latter process is most likely diffusion controlled, as repeating the experiments at 500 °C indicated that a relatively greater amount of chromium oxide was produced.

It is suspected that the chromium particles, once removed from the furnace, are stabilised by a thin unreactive oxide layer. This was highlighted in further experiments with hydrogen sulfide gas, which found that particles removed from the furnace and exposed to air were reluctant to undergo additional reactions to form sulfides, whereas particles which had not been removed from the furnace were found to successfully react further, producing chromium sulfides. However, if a stabilising oxide coat is present, it must be only a few atoms thick, as such a coat could not be readily observed on the particles in HRTEM images.

Chromium–nickel nanoparticles

Chromium–nickel alloy nanoparticles on silica with metal stoichiometries of Ni_2Cr, CrNi and Cr_2Ni were prepared *via* a similar process to that used for the chromium particles. The EDX data for the products show a wide range of compositions in each sample, for example, the CrNi preparation contained particles as nickel-rich as $Ni_{0.9}Cr_{0.1}$ and as chromium-rich as $Cr_{0.9}Ni_{0.1}$. Two electron micrographs of particles are shown in Fig. 6 and 7. From measurements on over 50 particles, the average particle size from electron microscope observations was approximately 15 nm, with a size variation of 2 to 30 nm.

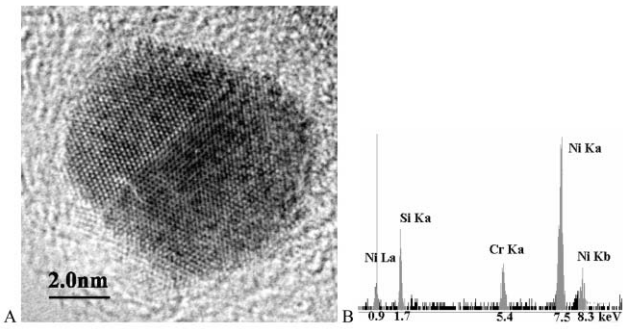

Fig. 6 An HRTEM image of a twinned Ni–Cr alloy nanoparticle of size 7 nm (A). A face-centred cubic structure is adopted. The composition obtained from the EDX spectrum (B) was $Ni_{0.72}Cr_{0.28}$.

In the nickel–chromium system, the alloy adopts a face-centred cubic (f.c.c.) arrangement of atoms at the nickel-rich end and a body-centred cubic (b.c.c.) arrangement at the chromium-rich end, between these is a region where both phases co-exist.[22] It was found in this study that the nanoparticles did indeed conform to this distribution. Although many of the nanoparticles were twinned, such as that shown in Fig. 6, no particles were found with what could be identified as an f.c.c. domain and a b.c.c. domain, with all particles observed being invariably of one structure type or the other. Interestingly, one particle, shown in Fig. 7, displayed a pronounced superstructure. The nickel chromium system contains a low-temperature ordered phase, Ni_2Cr, which also displays a superstructure. This phase results from a lattice contraction of a disordered f.c.c. matrix changing into an orthorhombic phase.[23,24] It is possible that the nanocrystal in Fig. 7 is adopting this phase, however EDX analysis indicated a composition closer to Cr_2Ni rather than Ni_2Cr. If this is indeed the true composition, then this would suggest the possibility of other phases in the chromium–nickel system containing superlattices. Despite the large numbers of particles investigated, this was the only one found showing a superlattice and cannot therefore be regarded as significant in the preparation. As in the case of the chromium nanoparticles, energy dispersive spectroscopy X-ray spectra were recorded from several areas of the silica support where no particles were present. Some of these spectra showed the presence of varying amounts of chromium and nickel in the support, and so the compositions obtained from nanocrystals on this support must be treated with some caution.

PXRD patterns for the chromium and chromium–nickel preparations contained no discernable peaks, which may be attributed to both the relatively low concentration of particles and the small particle size. The concentration of nanocrystallites in the sample proved difficult to accurately judge, although by comparison with specimens of nickel nanoparticles, it appeared to be very small, approximately 10 to 20%. For the chromium metal and chromium–nickel samples EDX spectra from areas of the silica support which had no observable metal particles still showed peaks due to the presence of chromium or chromium and nickel, indicating that, despite the high loadings (50% molar loadings), the metal was monodispersed on the support surface and probably absorbed into the bulk. This would account for the reduction in the concentration of nanoparticles actually observed. In addition, the average particle size from observations in the electron microscope was found to be particularly small, with many particles as small as 2 nm across. This small size will lead to a broadening of the diffraction peaks, which, in this case, probably become so broad that they would ordinarily be quite difficult to detect, even if large numbers of nanoparticles were present.

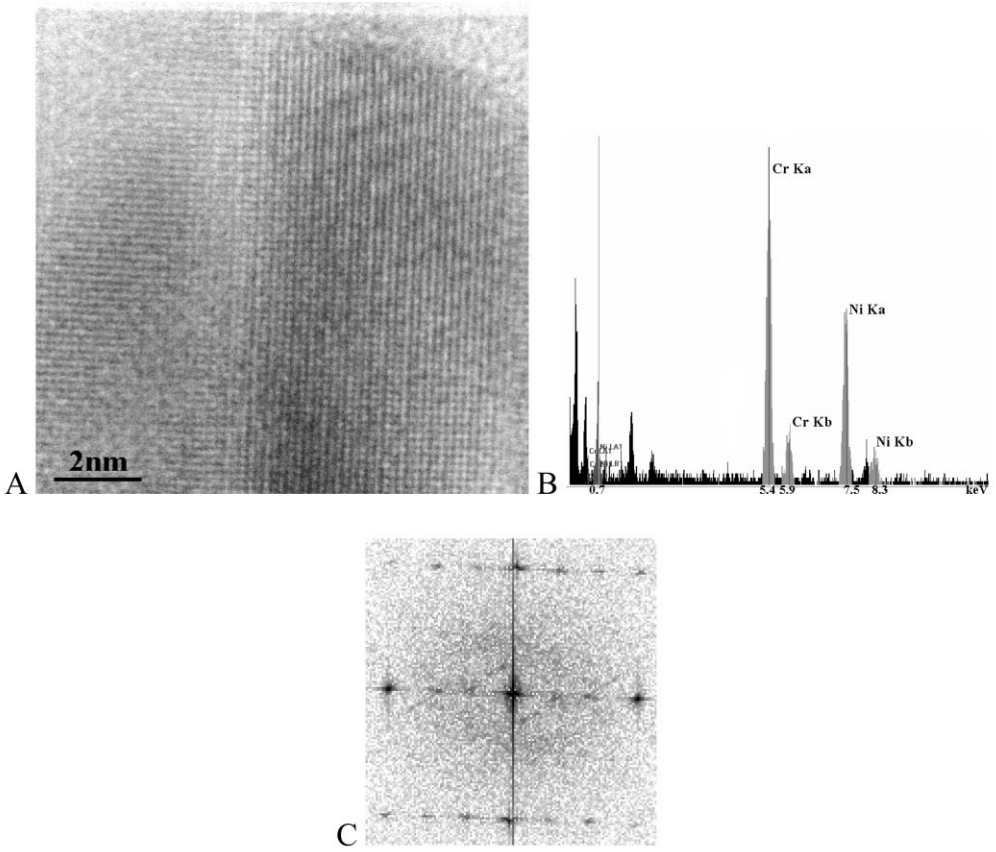

Fig. 7 An HRTEM image of a 15 nm chromium–nickel alloy nanoparticle (A). The EDX spectrum (B) gave a composition of $Cr_{0.68}Ni_{0.32}$. The power spectrum (C) contains additional spots, indicating the presence of a superstructure and additional ordering.

Conclusions

Nickel nanocrystals have been synthesised on graphitised carbon, ceria and alumina supports. The supports were found to have little effect on the average particle size but had a noticeable influence on morphology, with particles on alumina being found to adopt flat, angular shapes compared to those on graphitised carbon and ceria which had pseudo-spherical morphologies. The successful synthesis of chromium and chromium–nickel nanocrystals was achieved by the use of non-aqueous solvents. HREM studies of the particles showed that, in both cases, the structure types adopted were similar to those of the bulk phases and that the morphologies were pseudo-spherical. Methods for the solution synthesis of metal nanoparticles and nanoparticles of alloys of metals to the left of the periodic table are few in number and the approaches used in this report can be exploited for possible synthesis of numerous new metal and metal alloy nanoparticles with potential applications as catalysts and synthetic precursors.

Acknowledgements

We would like to thank the EPSRC for funding this research. Financial support for R. D. T. was also obtained from JEOL (UK) Ltd. and the Isaac Newton Trust, and this is gratefully acknowledged.

References

1 C. B. Murray, S. Sun, H. Doyle and T. Betley, *MRS Bull.*, 2001, **26**, 985.
2 V. F. Puntas, K. M. Krishnan and A. P. Alivisatos, *Science*, 2001, **291**, 2115.
3 S. Illy, O. Tillement, F. Machizaud, J. M. Dubios, F. Massicot, Y. Fort and J. Ghanbaja, *Philos. Mag. A*, 1999, **79**, 1021.
4 J. Walter, *Adv. Mater.*, 2000, **12**, 31.
5 A. Ueno, H. Suzuki and Y. Kotera, *J. Chem. Soc., Faraday Trans. 1*, 1983, **79**, 127.
6 S. Fujita, N. Hiyoshima and N. Takezawa, *React. Kinet. Catal. Lett.*, 1999, **67**, 9.
7 O. Yokata, Y. Oku, T. Sano and M. Tsuji, *Int. J. Hydrogen Energy*, 2000, **25**, 81.
8 D. Li, A. Nishijima and D. E. Morris, *J. Catal.*, 1999, **182**, 339.
9 H. Tamagawa, K. Oyama, T. Yamaguichi, H. Tanaka, H. Tsuki and A. Ueno, *J. Chem. Soc., Faraday Trans. 1*, 1987, **83**, 3189.
10 C. Estournez, T. Lutz, J. Happich, T. Quaranta, P. Wissler and J. L. Guille, *J. Magn. Magn. Mater.*, 1997, **173**, 83.
11 R. Monaci, A. Musinu, G. Piccaluga and G. Pinna, *Mater. Sci. Forum*, 1995, **195**, 1.
12 S. Ramesh, Y. Koltypin, R. Prozorov and A. Gedanken, *Chem. Mater.*, 1997, **9**, 546.
13 T. C. Rojas, M. J. Sayagues, A. Caballero, Y. Koltypin, A. Gedanken, L. Ponsonnet, B. Vacher, J. M. Martin and A. Fernandez, *J. Mater. Chem.*, 2000, **10**, 715.
14 J. B. Peri, *J. Catal.*, 1984, **86**, 84.
15 W. J. J. Welters, G. Vorbeck, H. W. Zandbergen, J. W. de Haan and R. A. van Santen, *J. Catal.*, 1994, **150**, 155.
16 J. Merida-Robles, P. Oliver-Pastor, E. Rodriguez-castellon and A. Jimenez-Lopez, *J. Catal.*, 1997, **169**, 317.
17 R. Cid, P. Atanasova, R. Lopez-Cordero, J. M. Palacios and A. Lopez-Agudo, *J. Catal.*, 1999, **182**, 328.
18 M. Green and P. O'Brien, *Chem. Commun.*, **2001**, 1912.
19 S. Sun, C. B. Murray, D. Weller, L. Folks and A. Moser, *Science*, 2000, **287**, 1989.
20 D. G. Mustard and C. H. Bartholomew, *J. Catal.*, 1981, **67**, 186.
21 C. H. Bartholomew, R. B. Pannell and J. L. Butler, *J. Catal.*, 1980, **65**, 335.
22 P. Nash, in *Binary Alloy Phase Diagrams*, ed. T. B. Massalski, ASM International, Materials Park, OH, 2nd edn., 1990, p 1031.
23 L. Karmazin, *Mater. Sci. Eng.*, 1982, **54**, 247.
24 A. Marucco, *J. Mater. Sci.*, 1995, **30**, 4188.